



# Antiaging activity, molecular docking, and prediction of percutaneous absorption parameters of quinoline–hydrazone hybrids

Edison Osorio <sup>1</sup> · Karent Bravo<sup>1</sup> · Wilson Cardona<sup>2</sup> · Andres Yepes<sup>2</sup> · Edison H. Osorio<sup>3</sup> · Juan C. Coa<sup>2</sup>

Received: 6 March 2019 / Accepted: 16 August 2019  
© Springer Science+Business Media, LLC, part of Springer Nature 2019

## Abstract

The application of antiaging agents can contribute to the prevention and control of skin photoaging. In the current research, nine quinoline–hydrazone hybrids were synthesized to obtain biologically active compounds as possible antiaging agents. The compounds were tested through a comprehensive in vitro evaluation of antielastase, anticollagenase, and antihyaluronidase activities along with the determination of their potential to quench reactive oxygen species (ROS) by the ORAC method. The selected hybrids were subsequently tested on human dermal fibroblasts (HDF) to reveal possible UVB photoprotective activity. The most potent antiaging protection of all the prepared compounds was shown by the trihydroxylated quinoline–hydrazones **5** and **9**, which showed the best collagenase inhibition ( $IC_{50} = 39.4$  and  $45.6 \mu M$ , respectively). Compound **5** also showed activity against elastase and hyaluronidase ( $IC_{50} = 164.2$  and  $318.8 \mu M$ , respectively). The molecular docking results suggest that the difference of inhibition between **5** and **9** is principally attributed to the hydrogen bonds interactions in the residues His218 and His228, and Zn atom in collagenase, Val216 in elastase and Tyr75 in hyaluronidase. In addition, compounds **5** and **9** were able to significantly protect human skin cells from UVB radiation in vitro. These compounds significantly decreased UVB-induced MMP-1 and ROS production and inhibited the suppression of type I procollagen synthesis in cultured HDF. The in silico dermatopharmacokinetic parameters showed promising results. Therefore, our study presented promising results for antiaging drug discovery, focusing on quinoline–hydrazone hybrids as dual inhibitors of skin aging-related enzymes, antioxidants, and inhibitors of the biological effects of UVB irradiation.

**Keywords** Quinoline–hydrazone hybrids · UVB photoprotection · Antiaging · Matrix metalloproteinase · Human dermal fibroblasts

**Supplementary information** The online version of this article (<https://doi.org/10.1007/s00044-019-02427-0>) contains supplementary material, which is available to authorized users.

- ✉ Edison Osorio  
edison.osorio@udea.edu.co
- ✉ Wilson Cardona  
wilson.cardona1@udea.edu.co

- <sup>1</sup> Grupo de Investigación en Sustancias Bioactivas, Facultad de Ciencias Farmacéuticas y Alimentarias, Universidad de Antioquia, Calle 70 No., Medellín 52-21, Colombia
- <sup>2</sup> Química de Plantas Colombianas, Instituto de Química, Universidad de Antioquia, Calle 70 No., Medellín 52-21, Colombia
- <sup>3</sup> Facultad de Ciencias Naturales y Matemáticas, Universidad de Ibagué, Carrera 22 calle 67, Ibagué, Colombia

## Introduction

The extracellular matrix (ECM) is the largest component of the dermis and provides the structural framework essential for the growth and elasticity of the skin. The ECM is composed of proteoglycans interwoven with macromolecules, such as collagen, elastin, and fibronectin, which are produced by the fibroblasts of the dermis (Duque et al. 2017). Collagen is the most abundant protein in the ECM and is responsible for the elasticity and strength of the skin and for maintaining its flexibility (Ndlovu et al. 2013). Elastin is an important protein with the unique property of elastic recoil, which is vital to maintaining skin elasticity and resilience, while hyaluronic acid (HA), a major glycosaminoglycan, is involved in the hydration of the skin, holding water and keeping the body smooth, moist, and

lubricated (Bravo et al. 2016). These connective tissue macromolecules are constantly attacked by enzymes such as matrix metalloproteinases (MMPs; e.g., collagenase), the serine protease elastase and the mucopolysaccharase hyaluronidase, which are highly related to the aging process of the skin (Duque et al. 2017). The extrinsic skin aging process (also called skin photoaging) occurs as a result of exposure to environmental factors, particularly solar radiation (UV radiation), which affects human skin in different ways. UV irradiation results in important molecular changes, including altered signal transduction pathways that promote MMP expression, decreased procollagen synthesis, connective tissue damage and significantly increased reactive oxygen species (ROS) (Freitas-Rodríguez et al. 2017). ROS can initiate complex molecular pathways, including the activation of enzymes, such as collagenase, elastase, and hyaluronidase (Bravo et al. 2016). Therefore, skin aging is a multifactorial and complex process. The induction of MMP expression through different pathways that are directly stimulated by UV irradiation contributes to the photoaging processes occurring in dermal ECM (Freitas-Rodríguez et al. 2017). Therefore, the exploration of strategies to combat the devastating effects of photoaging should focus on the different mechanisms involved in its pathogenesis.

Several investigations have shown that there are a number of chemicals derived from nature, in addition to a number of synthetic drugs, with varied therapeutic effects that may be useful in the control of the process of aging or photoaging (Mukherjee et al. 2011; Ndlovu et al. 2013). In the vast majority of cases, these molecules act on a specific target. However, factors such as low pharmacokinetic profiles, drug–drug interactions, poor solubility, and low stability are responsible for the insufficient effectiveness of single target-directed drug therapies (Choudhary et al. 2018; Hohl et al. 2001). It has also become apparent in recent years that many natural small compounds act on more than one particular target in the multidimensional process of aging (Cătană et al. 2018), or similar to integrated strategies, different compounds in natural extracts have been one of the main strategies used to decelerate and prevent the effects of skin aging (Duque et al. 2017; Mukherjee et al. 2015). Many herbs have been reported to contain bioactive metabolites, mainly polyphenolic compounds with photoprotective and antioxidant effects, which interact with cellular signaling pathways that are directly involved in the skin (Duque et al. 2017). Although the search for effective, nontoxic natural compounds with antiaging activity has been intensified in recent years, one of the strategies that is employed to treat these multifactorial processes but that is little explored in photoaging is related to the design of ligands comprising two pharmacophores in a single biological molecule that modulates multiple targets. The design of natural product-based hybrid molecules has emerged as a

robust approach involving a combination of two or more biologically active compounds of natural origins and allowing the simultaneous delivery of these compounds to target organs. This hybrid approach has been reported to possess a distinct advantage over the conventional approach of the coadministration of single target molecules due to better long-term prognosis and reduced toxicity. In addition, hybrid molecules result in enhanced dosage compliance, the reduction of drug–drug interactions and cheaper preclinical evaluation (Choudhary et al. 2018).

Hydrazones constitute an important type of biologically active compound with beneficial effects against different diseases (Singh and Raghav 2011; Verma et al. 2014). Furthermore, many reports have also verified that hydrazones present anticancer (Yadagiri et al. 2014), anti-inflammatory (Kumar et al. 2015), antiviral (Şenkardes et al. 2016), antiprotozoal (Coa et al. 2015; Vergara et al. 2017), and antibacterial activities (Popiołek 2017). Bioactive hydrazones bearing antioxidant groups represent an interesting approach towards the development of antiaging compounds. In fact, a number of hydrazones have been found to be powerful antioxidants. Hydrazones have exhibited good antioxidant power using the thiobarbituric acid reactive substances method, with interesting effects on superoxide radical scavenging and the inhibition of copper-induced and UV-induced LDL oxidation (Belkheiri et al. 2010; Yılmaz et al. 2012). In addition, the inhibition of the activity of ECM-degrading enzymes or protection against UV irradiation may be a useful approach to prevent photoaging. In this sense, hydrazones have been reported for their antielastase activity ( $IC_{50} = 21.1 \mu M$ ) (Nurkenov et al. 2017), and the possible application of hydrazones as UV absorbers in the pharmaceutical and cosmetic industry has been reported (Dimitrijević et al. 2016). However, a quinolinic core is a structural feature of several bioactive compounds. Thus, this core is an interesting constituent for new drug design. Antimycobacterial, antimicrobial, anticonvulsant, antiinflammatory, antitumoral, cardiovascular, and antiprotozoal are some of the biological activities exhibited by compounds having this heteroaromatic ring (Coa et al. 2017; Franck et al. 2004; Suresh et al. 2009). In relation to its antiaging potential, a pyrroloquinoline quinone has shown a protective effect on UVA irradiation-induced human dermal fibroblasts (HDF) (Zhang et al. 2015). Another compound of this type presented high inhibitory activity towards hyaluronidase ( $IC_{50} = 579.77 \pm 16.28 \mu M$ ) (Czarnecka et al. 2017). Based on the aforementioned characteristics, a series of synthetic quinoline–hydrazone hybrids (Coa et al. 2015) were evaluated for their antiaging activities. The compounds were evaluated by their capacity to inhibit the collagenase, elastase, and hyaluronidase enzymes, by their antioxidant properties and by their protective effects against the damage

induced by UVB radiation in HDF. In addition, molecular docking has been reported as an effective method to predicting the impact of biomolecules on skin photoaging (Farrokhnia, Mahnam 2017; Sivamani et al. 2012; Zeng et al. 2016). To improve our understanding of the protective role of different hydrazones against photoaging, the molecular interactions between hydrazones and elastase and hyaluronidase enzymes were analyzed through molecular docking.

## Experimental

### In vitro determination of antiaging properties

The antiaging properties of molecules were measured by their capacity to inhibit the activity of skin aging-related enzymes, following previously reported assays (Bravo et al. 2016). For compounds with higher activity, the  $IC_{50}$  values were determined.

### Anticollagenase activity

The inhibition of collagenase enzyme was measured using the EnzCheck® Gelatinase/Collagenase assay kit (Molecular Probes Inc.). Aliquots of 20  $\mu$ L of 500  $\mu$ M sample solutions or buffer (control) were added to each well of a 96-well plate. Then, 80  $\mu$ L of DQ-collagen type IV substrate followed by 100  $\mu$ L of active enzyme were added, and the fluorescence intensity was measured by a Synergy HT Multi-Mode Microplate Reader (BioTek Instruments, Inc.; Winooski, USA) at an excitation of 485 nm and emission detection of 515 nm at each minute for 20 min. Oleanolic acid (250  $\mu$ M) was used as a reference inhibitor. Each reaction was performed in triplicate. The percent inhibition of the collagenase reaction was calculated using Eq. (1).

$$\text{Inhibition (\%)} = M_{\text{Control}} - M_{\text{Sample}} M_{\text{Control}} \times 100 \quad (1)$$

where  $M_{\text{Control}}$  and  $M_{\text{Sample}}$  are the slopes of the fluorescence vs time graph for the control and the sample, respectively.

### Antielastase activity

The effect on elastase enzyme was measured using the EnzCheck® Elastase assay kit (Molecular Probes Inc.). Aliquots of 50  $\mu$ L of 500  $\mu$ M sample solutions or buffer (control) were added to each well of a 96-well plate. Then, 50  $\mu$ L of DQ-elastase substrate and 100  $\mu$ L of active enzyme were added. The fluorescence intensity was measured under the conditions described for the previous assay. Oleanolic acid (250  $\mu$ M) was used as a reference inhibitor. Each reaction was performed in triplicate. The percent inhibition of the elastase reaction was calculated using Eq. (1).

### Antihyaluronidase activity

Briefly, 30  $\mu$ L of sodium phosphate buffer (20 mM, pH 7.0) with sodium chloride (77 mM) and bovine serum albumin-BSA (0.01%, control) or 250  $\mu$ M sample solution dissolved in the same buffer were incubated for 45 min at 37 °C in a water bath with 90  $\mu$ L of hyaluronidase from the bovine test, prepared in the above buffer and 120  $\mu$ L of HA sodium salt (300 mM) in sodium phosphate buffer at pH 5.35. Next, 100  $\mu$ L of reaction mix containing undigested HA was precipitated with 500  $\mu$ L of acid albumin solution, made up of bovine serum albumin (0.1%) in sodium acetate (24 mM) and acetic acid (79 mM, pH 3.75). The mixture was allowed to stand at room temperature for 10 min, and then the absorbance was measured at 600 nm. Epigallocatechin gallate (250  $\mu$ M; EGCG) was used as a reference inhibitor. The control vial with complete reaction was considered to be 100% enzyme activity (EA), and a control substrate, where the enzyme solution was replaced by 90  $\mu$ L of the buffer, was considered not active. The percent inhibition of the hyaluronidase reaction was calculated as follows:

$$\text{Inhibition (\%)} = 1 - EA_{\text{sample}} EA_{\text{control}} \times 100 \quad (2)$$

where  $EA_{\text{sample}}$  and  $EA_{\text{control}}$  are the enzyme activities of the sample and control, respectively.

The enzyme activity parameter was calculated as follows:

$$\text{Enzyme activity (\%)} = 100\% - [A_{600 \text{ nm}}^{\text{sample}} A_{600 \text{ nm}}^{\text{substrate}} \times 100] \quad (3)$$

where the  $A_{600 \text{ nm}}^{\text{sample}}$  is the absorbance at 600 nm of the reaction with sample, and the  $A_{600 \text{ nm}}^{\text{substrate}}$  is the absorbance at 600 nm of the reaction without enzyme solution (control substrate).

### Antioxidant properties

The antioxidant capacity of the compounds was measured by a hydrophilic oxygen radical absorbance capacity (ORAC) assay following a previously described procedure (Bravo et al. 2015), and using a Synergy HT Multi-Mode Microplate Reader (BioTek Instruments, Inc.; Winooski, USA). Then, 25  $\mu$ L of sample solution or Trolox standard was mixed with 150  $\mu$ L of 1  $\mu$ M fluorescein and pre-incubated at 37 °C for 30 min. Then, 25  $\mu$ L of 200 mM AAPH (2,2'-azobis(2-amidinopropane) dihydrochloride) was added. The fluorescence at an excitation wavelength of 485 nm and an emission wavelength of 520 nm was measured every 2 min for 120 min. The quantification of antioxidant activity was based on the calculation of the area under the fluorescence curve using the Trolox standard

(Prior et al. 2005). The results are expressed as  $\mu\text{mol TE/g}$  of compound.

### Photoprotective effects in human dermal fibroblasts (HDF)

The photoprotective effects on HDF of the quinoline–hydrazone hybrids active as aging-related enzyme inhibitors were measured by their modulation of MMP-1, procollagen, and ROS production after UVB exposure (Bravo et al. 2017). HDF from adult skin (HDFa) and material for their maintenance and culture were obtained from Life Technologies Inc. (USA). During assays, HDFa in 3rd to 4th passages were maintained in DMEM-F12 GlutaMAX™ supplemented with 10% heat-inactivated fetal bovine serum (FBS), 100 U/mL penicillin and 100  $\mu\text{g/mL}$  streptomycin in a humidified atmosphere of 5%  $\text{CO}_2$  at 37 °C. The cells were cultivated in 75 mL culture flasks until they reached 90% confluence. Then, HDFa were plated in 96-well plates where different assays were performed. During the tests, the cells were irradiated using a UV Irradiation System for Cultures (Vilber Lourmat, Marne, France).

### Cell viability

Cell viability was measured using the highly water-soluble tetrazolium salt WST-8 (2-(2-methoxy-4-nitrophenyl)-3-(4-nitrophenyl)-5-(2,4-disulfophenyl)-2H-tetrazolium) contained in Cell Counting Kit-8 (Dojindo Molecular Technologies, Inc., Rockville, MD, USA) and following the manufacturer's instructions. The cells were plated in 96-well plates at a density of  $10^4$  cells/well. For this assay, 200  $\mu\text{L}$  of  $5 \times 10^4$  cells/mL in supplemented medium was cultured overnight. Then, the medium was removed, and the cells were treated with various concentrations of compounds (1, 5, 10, 50, 100, and 250  $\mu\text{M}$ ) dissolved in 100  $\mu\text{L}$  of FBS-free medium for 24 h. The cells were washed with PBS and 100  $\mu\text{L}$  of FBS-free medium, and then 10  $\mu\text{L}$  of WST-8 was added. Finally, the absorbance was measured at 450 nm using a multimode microplate reader (BioTek Instruments, Inc., Winooski, USA).

### Effects on MMP-1 and procollagen production

The MMP-1 and procollagen production in HDFa after UVB exposure was measured by ELISA using the commercial kits Human Total MMP-1 DuoSet and Human Procollagen I alpha 1 DuoSet (R&D Systems, Inc., Minneapolis, USA), according to the manufacturer's instructions and following the conditions in previously reports (Bravo et al. 2017). Briefly, HDFa were plated at a density of  $10^4$  cells/well in 96-well plates in 200  $\mu\text{L}$  of

supplemented medium overnight. Then, the medium was removed, and the cells were treated with 2, 10, and 50  $\mu\text{M}$  compounds dissolved in 100  $\mu\text{L}$  of FBS-free medium for 24 h. The samples were removed, and the cells were washed twice with PBS. Then, 100  $\mu\text{L}$  of FBS-free medium was added, and the plates were exposed to 100  $\text{mJ/cm}^2$  UVB. After irradiation, the cells were incubated at 37 °C. At 24 and 72 h postirradiation, the supernatants were collected for the MMP-1 and procollagen assays, respectively. A total of 25  $\mu\text{M}$  EGCG was used as a reference compound in the MMP-1 production assay, and 25  $\mu\text{M}$  ascorbic acid was used as a reference compound in the procollagen production assay.

### Effects on ROS production

The effect of compounds on ROS production in HDFa induced by UVB was measured using 2',7'-dichlorofluorescein diacetate (DCFH-DA; Molecular Probes Inc., Eugene, OR, USA) and following previously described procedures (Bravo et al. 2017). HDFa were plated at a density of  $5 \times 10^4$  cells/well in black 96-well plates in 200  $\mu\text{L}$  of supplemented medium overnight. The medium was removed, and the cells were treated with 2, 10, and 50  $\mu\text{M}$  compounds dissolved in 100  $\mu\text{L}$  of FBS-free medium for 2 h. Then, 10  $\mu\text{L}$  of 250  $\mu\text{M}$  DCFH-DA was added and incubated at 37 °C for 30 min. The plates were exposed to 200  $\text{mJ/cm}^2$  UVB. After 30 min, the samples were removed, and 100  $\mu\text{L}$  of FBS-free medium was added. Finally, the fluorescence was read at the excitation and emission wavelengths of 485 and 520 nm, respectively. Quercetin (25  $\mu\text{M}$ ) was used as a reference antioxidant.

### Molecular docking

The molecular docking studies were performed to investigate the binding mode into the active site of three different enzymes, fibroblast collagenase, native porcine pancreatic elastase and human hyaluronidase, PDB Codes 1CGL (Lovejoy et al. 1994), 1QNJ (Würtele et al. 2000), and 2PE4 (Chao et al. 2007), respectively. The information about the experimental resolution of each protein could be consulted in the Protein Data Bank web site. The three-dimensional (3D) structures of compounds or ligands were submitted to a geometrical optimization procedure at PBE0 (Adamo and Barone 1999) /6–311 + g\* level of theory using the Gaussian 09 program (Frisch et al. 2009; Newton 1969). All optimized conformations were confirmed as a minimum on the potential energy surface.

The docking simulations for the set of optimized ligands were performed using the AutoDock v.4.2 program (Morris et al. 2009). AutoDock combines a rapid energy evaluation through precalculated grids of affinity potentials with a

variety of search algorithm to find suitable binding positions for a ligand on a given macromolecule. This program performs global searches by incorporating the van der Waals attractive potential, geometric collision, screened electrostatic potential, and Lazaridis–Karplus desolvation energy into the scoring function. Therefore, all molecular docking results presented in this work are global Docking. In the preparation of the enzymes for docking simulations the water molecules, cofactors, and ions were excluded from each X-ray crystallographic structure. Only in the fibroblast collagenase, the Zinc atoms were conserved due to those belongs to the active site. Likewise, the polar hydrogen atoms of the enzymes were added, the atomic charges were computed toward the Gasteiger procedure and the nonpolar hydrogen atoms were merged. Finally, the enzyme was treated as a rigid body.

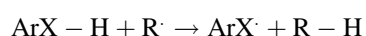
The molecular docking calculations were carried out in the active site of each protein. In the case of fibroblast collagenase, 1CGL, the box is centered on the original position of ligand crystalized, (*N*-[(1*s*)-3-[(benzyloxy) carbonyl] amino]-1-carboxypropyl]-1-leucyl-*N*-(2-morpholin-4-ylethyl)-1-phenylalaninamide) (OED) (Farrokhnia, Mahnam 2017). In the case of native porcine pancreatic elastase, 1QNJ, the active site was located around of Val 216 residue (Sivamani et al. 2012). Finally, in the human hyaluronidase, 2PE4, the active site was situated around of Tyr 75 residue, according to previously published works (Zeng et al. 2016).

Molecular docking normally requires a user-defined docking search space, where the possible ligand binding conformations are explored. A small search space can produce an insufficient number of conformations, while a generously large space could generate too many irrelevant interaction poses. Therefore, optimally confined docking search space is fundamental to the success of ligand–protein coupling. The default box size can be calculated using experimentally resolved protein–ligand complex structures. First, an initial box is constructed to enclose the ligand, and then the size of the box is increased in random directions to ensure that the minimum length in any dimension is at least 22.5 Å. The grid maps of interaction energy for various atom types with each macromolecule were calculated by the auxiliary program AutoGrid choosing a grid box centered at: (30.681, 46.555, −0.0090) for 1CGL, (16.203, 8.633, 1.518) for 1QNJ and (45.539, −21.778, −19.639) for 2PE4, with dimensions of 60 × 60 × 60 Å around the active site, and a grid point spacing of 0.375 Å. All these conditions are sufficiently to include the most important residues of each enzyme. The docking searches for the best orientations of the molecules to the active site of each protein were performed using the Lamarckian genetic algorithm (LGA) (Morris et al. 1998). The LGA protocol applied a population size of 2000 individuals, while 2,500,000 energy

evaluations were used for the 200 LGA runs. The best conformations were chosen from the lowest docked energy solutions in the cluster populated by the highest number of conformations. The best docking complex solutions (poses) were analyzed according to the potential intermolecular interactions (ligand/enzyme), such as hydrogen bonding, hydrophobic interactions, and the cation– $\pi$ ,  $\pi$ – $\pi$  stacking.

### In silico antioxidant evaluation

The mechanism used to evaluate theoretically the possible quenching of free radicals by the synthesized compounds was the hydrogen atom transfer (HAT) method, from the molecule to the radical (de Heer et al. 2000):



The electrophilicity index  $\omega$  was calculated as a measure for the capability of the radicals formed to acquire electronic charge from the environment (Parr et al. 1999). The spin density (SD) analysis (Parkinson et al. 1999), defined as the difference between  $\alpha$  and  $\beta$  electron densities, was evaluated as a local descriptor of stability. All calculations were performed at the PBE0/6–311 + g\* level of theory with the Gaussian 09 software package.

### In silico prediction of the pharmacokinetic properties and percutaneous absorption parameters

To determine the drug-like properties for all tested compounds 1–9, the physicochemical descriptors were determined using open-source cheminformatics toolkits such as the Molinspiration software (for MW, H-bond donors, H-bond acceptors, rotatable bonds, and TPSA descriptors) and ALOGPS 2.1 algorithm from the Virtual Computational Chemistry Laboratory (for  $\log P_{o/w}$  and aqueous solubility  $\log S_w$  descriptors). Furthermore, to obtain information on the kinetics of the adsorption and distribution required for skin permeability, four important dermatopharmacokinetic parameters were predicted for compounds 1–9. The skin permeation coefficient of chemical in the stratum corneum ( $\text{Log}K_p$ ) was calculated using PreADMET 2.0, and the percutaneous absorption ( $\text{Log}P_{ab}$ ) was predicted according to the equation [ $\text{Log}P_{ab} = -2.72 + 0.71 \times \text{Log} P_{o/w} - 0.0061 \times \text{MW}$ ]. The effective diffusion coefficient in human dermis ( $D_{de}$ ) was calculated using the equation [ $D_{de} = (7.1 \times 10^{-10}/\text{MW}^{0.5})$ ], and the most important parameter in determining the maximal dermal flux, toxicity, or systemic effect,  $J_{max}$ , was calculated using the equation [ $\text{Log} J_{max} = -3.90 - 0.0190 \times \text{MW}$ ]. These important parameters defining the penetration, absorption, permeation, movement, partitioning, and diffusion of the compounds have been applied to support the transdermal delivery of potential

drugs and skincare actives, as well as integrated risk assessment (Chen et al. 2015; Schoellhammer et al. 2014).

## Statistical analysis

All results are expressed as the mean  $\pm$  SD of three experiments. The statistical analyses were performed using GraphPad Prism 5 (GraphPad Software Inc., San Diego, CA, EUA). To evaluate significant ( $P < 0.05$ ) differences between compounds and controls, analysis of variance (ANOVA) was performed.

## Results and discussion

### Chemical synthesis

The synthesis and characterization of the compounds under study have already been published (Coa et al. 2015). The chemical structure of the hybrids evaluated is presented in Fig. 1. Quinaldine (A) was oxidized with selenium oxide to produce aldehyde B, which was treated with iodine and methanol in basic solution to afford ester C. Then, compound C was subjected to nucleophilic substitution with hydrazine hydrate to obtain acylhydrazide D, which was coupled with the different hydroxyaldehydes of E in aqueous medium to obtain hydrazones 1–5. Hydrazones 6–9 were obtained following the same synthetic strategy starting from 4-quinolinecarboxaldehyde (Fig. 1).

### In vitro antiaging properties and antioxidant capacity

The degradation of the ECM components induced by UVB stimulation might be among the main factors involved in skin photoaging (Mukherjee et al. 2015); therefore, the inhibition of collagenase, elastase, and hyaluronidase is an important antiaging target (Duque et al. 2017; Kumud and Sanju 2018). To develop a new class of inhibitors of skin aging-related enzymes, such as collagenase, elastase, and hyaluronidase, the synthetic quinoline–hydrazone hybrids 1–9 were evaluated as possible antiaging agents. The results are shown in Fig. 2. The best results, in terms of enzymatic inhibition, occurred when a high number of hydroxyl groups were present on the aromatic ring of hydrazone. The compounds with the best activity against collagenase and hyaluronidase were hybrids 5 and 9, which both have three hydroxylated positions (Fig. 2a, c). Hybrid 5 and the dihydroxy analog 7 showed elastase inhibition (Fig. 2b). The monohydroxy hybrid 1 was inactive or had slight activity, and the dihydroxybenzyl-hydrazone (2, 3, 4, 6, and 8) derivatives showed weak activity, establishing the importance of the positions of the hydroxyl groups (Fig. 2). The  $IC_{50}$  values were obtained for the more active compounds, and the results are shown in Table 1. Overall, the  $IC_{50}$  values were close to those determined for the reference compounds. However, in the inhibition of elastase, hybrid 5 showed better inhibition than the commercial standard oleanolic acid ( $IC_{50} = 193.6 \mu\text{M}$ ).

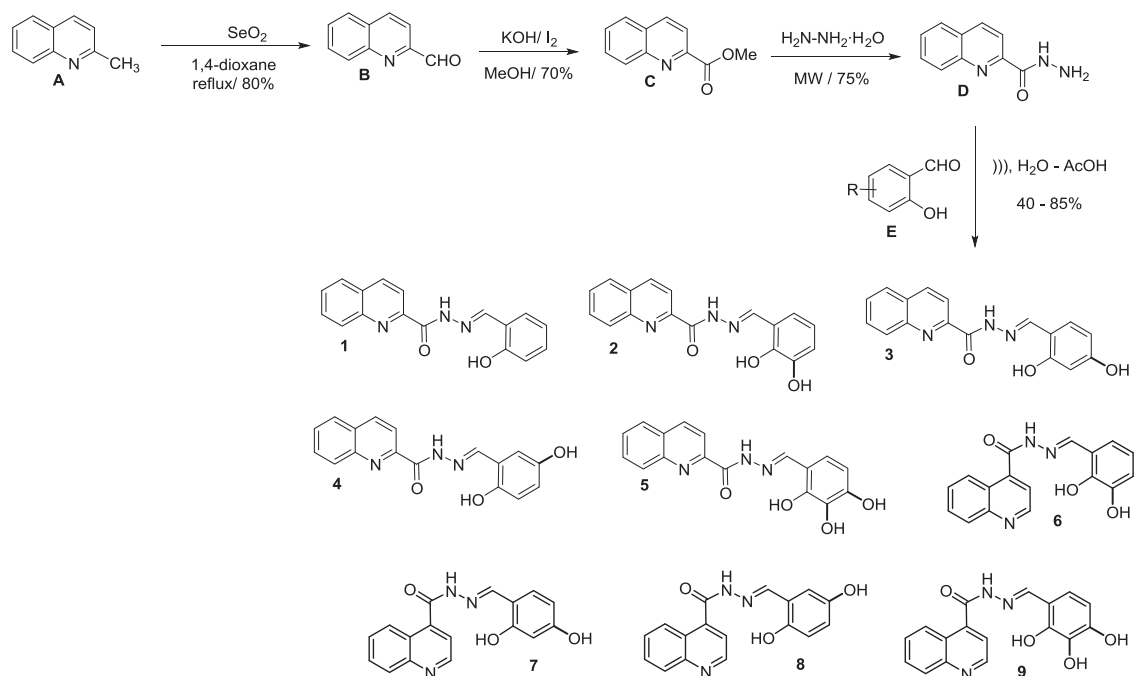
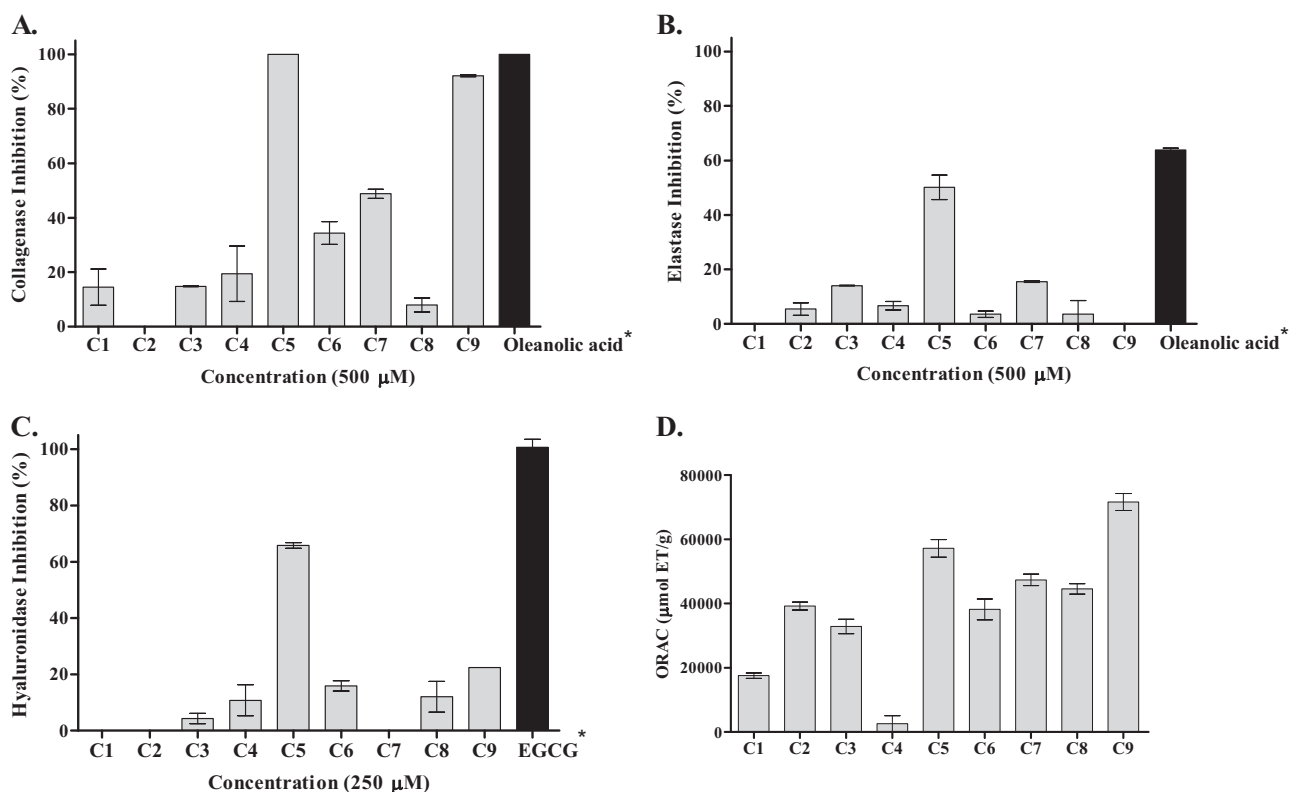


Fig. 1 The synthetic pathway of the quinoline–hydrazone hybrids



**Fig. 2** Effect of quinoline–hydrazone hybrids on skin aging-related enzymes and their antioxidant properties. Inhibitory activities (%) against **a** collagenase, **b** elastase, and **c** hyaluronidase. **d** The antioxidant activity as detected by the ORAC method, expressed as  $\mu\text{mol}$

TE/g compound. Bars are mean  $\pm$  standard deviation for three replicates. Asterisks indicate an evaluation concentration of 250  $\mu\text{M}$  (reference inhibitors)

**Table 1**  $\text{IC}_{50}$  ( $\mu\text{M}$ ) of more potential quinoline–hydrazone hybrids against aging-related skin enzymes

Compounds	Anticollagenase	Antielastase	Antihyaluronidase
<b>5</b>	$39.39 \pm 2.7$	$164.2 \pm 8.0$	$318.8 \pm 22.6$
<b>9</b>	$45.61 \pm 2.5$		
Oleanolic acid <sup>a</sup>	$29.98 \pm 1.8$	$193.6 \pm 8$	
EGCG <sup>b</sup>			$210.7 \pm 3.00$

<sup>a</sup>Oleanolic acid was used as a positive control for anticollagenase and antielastase activity

<sup>b</sup>EGCG was used as a positive control for antihyaluronidase activity

In order to propose a molecular level explanation on the enzymes elastase, collagenase, and hyaluronidase inhibition by the best inhibitors (quinoline–hydrazone hybrids **5**, **7**, and **9**), a molecular docking study was carried out assuming a model where the protein and ligand were considered as rigid and flexible, respectively, during the docking procedure. Unfortunately, the sameness in the estimated binding energy values, presented in Table 2, did not allow determine large differences in the inhibition between the synthesized compounds. A possible explanation could be the limitation of docking model for explains how the compounds could arrive to the active site. In all the molecular docking

**Table 2** Estimated free energy of binding for the quinoline–hydrazone hybrids expressed in  $\text{kcal mol}^{-1}$

Compounds	Anticollagenase	Antielastase	Antihyaluronidase
1	−7.65	−7.68	−7.73
2	−8.48	−7.59	−7.99
3	−8.03	−7.55	−7.67
4	−7.99	−7.36	−8.78
5	<b>−8.04</b>	<b>−7.19</b>	<b>−7.46</b>
6	−7.45	−7.27	−8.07
7	<b>−8.02</b>	<b>−7.64</b>	<b>−8.15</b>
8	−7.54	−7.25	−8.45
9	<b>−7.69</b>	<b>−7.45</b>	<b>−8.03</b>
Oleanolic acid <sup>a</sup>	−11.29	−7.64	
EGCG <sup>b</sup>			−9.45

<sup>a</sup>Oleanolic acid was used as a positive control for anticollagenase and antielastase activity

<sup>b</sup>EGCG was used as a positive control for antihyalurocollagenase activity

The bold values represent active and selected compounds for further studies

experiments, the procedure starts with the ligand located into the site active. However, a picture about the intermolecular interactions between protein and ligand should be

interesting for explain the difference in the inhibition between **5**, **7**, and **9** compounds. For that, graphical representations for the binding of ligand–collagenase, elastase, and hyaluronidase are present in the Fig. 3. The principal hydrogen bond interactions for the ligand–collagenase are: His218, His228, and His222 for oleanolic acid; His218, His228, Glu219, Ala184 for **5**, and finally Ala184 and Glu219 for **9**. In this case, the less stabilization of **9** can be explained for the absence of residues His218 and His228, and the not closeness with the Zn atom. In the case of the elastase–ligand complex, the principal hydrogen bond interactions are Val216, Thr41, and Arg61 for oleanolic acid; Ser214, Val216, and Ser217 for **5**; and Asn148, Gln192, Val216 for **7**. In all cases, the residue Val216 looks as important residue for the ligand stabilizations. Finally, the hydrogen bond interactions present for hyaluronidase–ligand complex are composed by Tyr75, Ser76, Tyr286, Ser323, and Trp324 for EGCG; Tyr75, Val322, and Thr327 for **5**; and Ser76, Asp129, Glu131 for **9**. In this case, the less stabilization of **9** could be explained, at least in part, for the absence of residues Tyr75. Information about the hydrophobic interactions for these ligand–protein complexes, can be seen in the Electronic Supplementary Information.

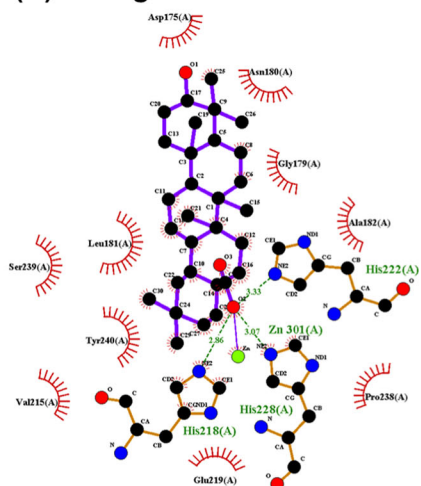
The evaluation of the antioxidant properties of the quinoline–hydrazone hybrids **1–9** studied in this work was performed by the ORAC method. The results are shown in Fig. 2d and are expressed as  $\mu\text{mol TE/g}$  of compound. The ORAC assay assessed the ability of compounds to scavenge peroxy radicals, which represent one of the contributors of lipid peroxidation. It is known that lipid radicals are formed when skin is exposed to UV. The major type of ROS produced on the surface of the skin is singlet oxygen ( $^1\text{O}_2$ ) (Ryu et al. 2009), which is oxidized to squalene, cholesterol, and unsaturated acyl residues in the sebum, yielding lipid-peroxy radicals. These ROS further oxidize proteins to produce carbonylated proteins in the stratum corneum (Masak 2010). Therefore, although lipid-peroxy radicals are very relevant, adducts detected in skin samples also correspond to dermal protein damage (mainly collagen and elastin) (Haywood et al. 2008). These data establish the importance of the peroxy radical scavenging capacity at the level of skin aging. From the screening of hybrids, it can be seen that the compounds with the best activity were the trihydroxybenzyl-hydrazone derivatives **5** and **9**. The dihydroxybenzyl analog **7** showed a slight reduction in antioxidant activity. The monohydroxy and dihydroxybenzyl hybrids **1** and **4** showed weak activity. Regarding the structure–activity relationship, it is interesting to note that, in general, as with enzymatic inhibition, as the number of hydroxyl groups increases in the molecule, the antioxidant capacity increases. In the dihydroxylated series (compounds **2–4** and **6–8**), it was observed that at the *meta*

and *para* oxygenated positions in the hybrids 2- and 4-quinoline–hydrazone are important for activity. In addition, the 4-quinoline–hydrazone hybrids (compounds **6–9**) show better antioxidant activity than the 2-quinoline–hydrazone series (compounds **1–5**). In fact, the position of the benzyl–hydrazone moiety on the quinoline ring of hybrid **8** led to an important improvement in activity compared with compound **4**.

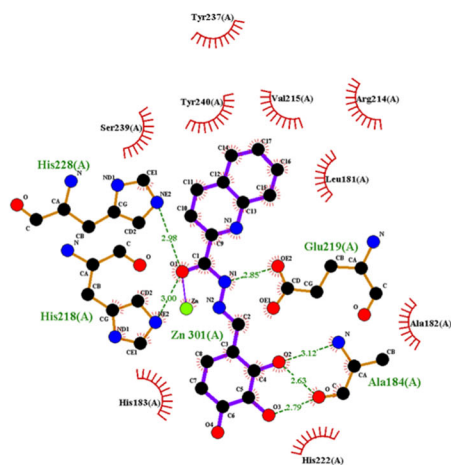
In order to understand the highest antioxidant activity of the hybrids **5** and **9**, the theoretical values for the bond dissociation enthalpy (BDE) of the homolytic cleavage N–H or O–H bonds, were calculated and are presented in Table 3. For HAT mechanism, a lower value of O–H BDE, calculated as  $BDE = [(ArX) + (H)] - [(ArX-H) + E(R)]$ , where E corresponds to energy, is indicative of an energetically process. The lowest values presented for the compounds **4**, **5**, **8**, and **9**, showed that the most favorable O–H bond homolytic cleavage is in meta positions. However, the electrophilicity index  $\omega$  show that the **5** and **9** radicals are the molecules with the highest capability to acquire electronic charge from the environment, allowing them to react with other potentially harmful radicals through specific hydrogen transfer mechanisms. These results can be confirmed by the electron density analysis for the **4**, **5**, **8**, and **9** radicals formed (Fig. 1. In Electronic Supplementary Information). Larger surfaces are indicative of stabilization of the respective radical species, and therefore to their persistence in the medium. Also, **5** and **9** compounds show two OH groups with a high probability to a posterior reaction, compared with **4** and **8**. So, these results show the efficacy of the potential antioxidant activity of the **5** and **9** hybrids.

Quinoline nuclei occur in several natural compounds and pharmacologically active substances, displaying a broad range of biological activities. In fact, the importance of the potent quinoline class of compounds has been established in the search for effective agents (Chaaban et al. 2018; El-Feky et al. 2015; Marella et al. 2013). In relation to its antiaging potential, some quinoline derivatives have been shown to possess antihyaluronidase activity (Czarnecka et al. 2017). Hydrazones are another class of biologically active moieties that are extensively explored as exhibiting various biological profiles (Singh and Raghav 2011; Verma et al. 2014). Derivatives of these compounds have exhibited potent antioxidant activity (Belkheiri et al. 2010; Yılmaz et al. 2012) and have been shown to be inhibitors of skin disease-related enzymes, mainly as antielastase agents (Nurkenov et al. 2017). However, despite this potential, there are no prior data available in the literature regarding the inhibition of skin disease-related enzymes of quinoline–hydrazone hybrids. Their very strong inhibition of collagenase, elastase, and hyaluronidase activities, particularly together with the potent antioxidant activity

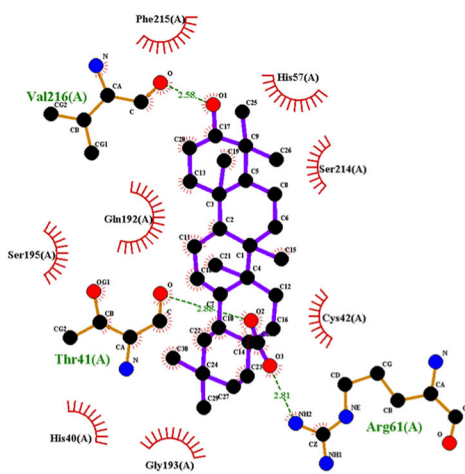
(A) Collagenase - Oleanolic Acid



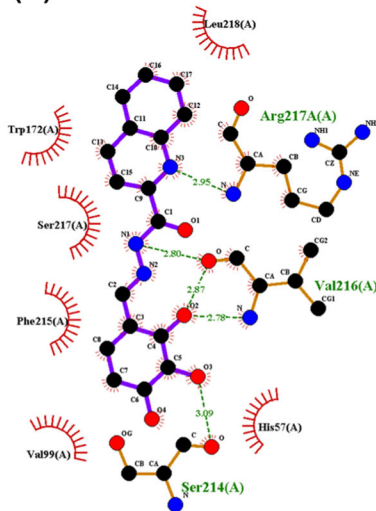
(B) Collagenase - C5



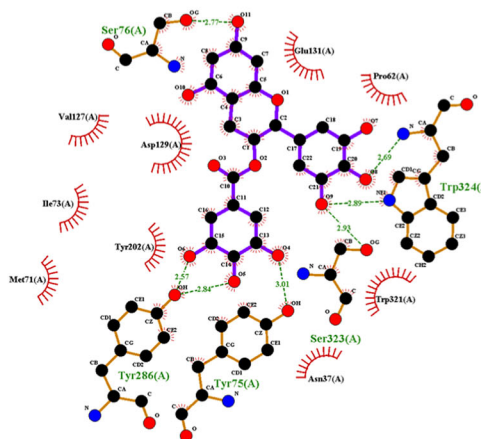
(C) Elastase - Oleanolic Acid



(D) Elastase - C5



(E) Hyaluronidase – EGCG



(F) Hyaluronidase – C5

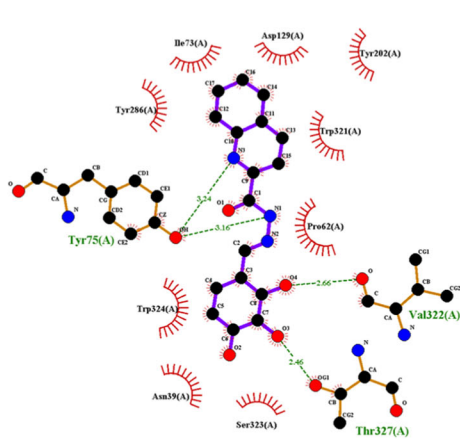


Fig. 3 Graphical representations for the binding of a collagenase–oleanolic acid; b collagenase–5; c elastase–oleanolic acid; d elastase–5; and e Hyaluronidase–EGCG

**Table 3** The bond dissociation enthalpy (BDE) and the electrophilicity index ( $\omega$ ) of the synthesized hybrids by HAT mechanism

Compounds	BDE for the radicals formed (kcal mol <sup>-1</sup> )				$\omega^a$ (kcal mol <sup>-1</sup> )
	N-H	OH, ortho	OH, meta	OH, para	
1	84.8	95.9	–	–	
2	84.9	87.9	85.6	–	
3	83.0	96.0	–	84.2	
4	84.4	91.3	<b>77.9</b>	–	16.4
5	82.9	89.8	<b>78.1</b>	83.9	<b>14.0</b>
6	89.9	84.0	85.6	–	
7	88.1	91.7	–	84.5	
8	89.5	87.0	<b>78.9</b>	–	16.1
9	88.0	86.0	<b>78.1</b>	84.3	<b>15.4</b>

<sup>a</sup>Reactivity descriptor for the OH-meta radicals formed

presented by some of the prepared hybrids, establishes that the occurrence of the quinoline hydrazone moiety has tremendously enhanced the antiaging activity. The test hybrids **5**, **7**, and **9** showed similar or even higher activity compared with the reference standards EGCG and oleanolic acid. Encouraged by these findings, it was interesting to synthesize and evaluate the biological activity of some of the structure hybrids that include a quinoline backbone bearing a substituted hydrazone moiety, aiming to highlight the potential of derivatives as a template for the development of antiaging and antioxidant agents with a diverse mechanisms of action.

### Photoprotective effect in human dermal fibroblasts (HDF)

The skin is the most exposed organ to ultraviolet (UV) irradiation, which induces premature skin aging. This type of aging (photoaging) is characterized by rough texture, coarse wrinkles, and mottled pigmentation (Kang et al. 2017). Although skin aging-related enzymes are expressed at low levels in unstimulated cells, UV irradiation results in important molecular changes, including the promotion of MMP-1 (fibroblast collagenase) expression, reducing the transcription of COL3a1 and COL1a1 genes, which encode procollagen I and III, causing connective tissue damage and significantly increasing ROS (Freitas-Rodríguez et al. 2017). Since MMP-1 induced by ROS causes collagen and elastin degradation, its inhibition and the promotion of collagen type I synthesis from procollagen type I are important targets for skin photoaging control and wrinkle prevention (Bravo et al. 2017). In this study, the modulation of HDF of MMP-1, procollagen and ROS production in UVB-mediated skin photoaging by trihydroxybenzylhydrazone derivatives **5** and **9** was examined. The results

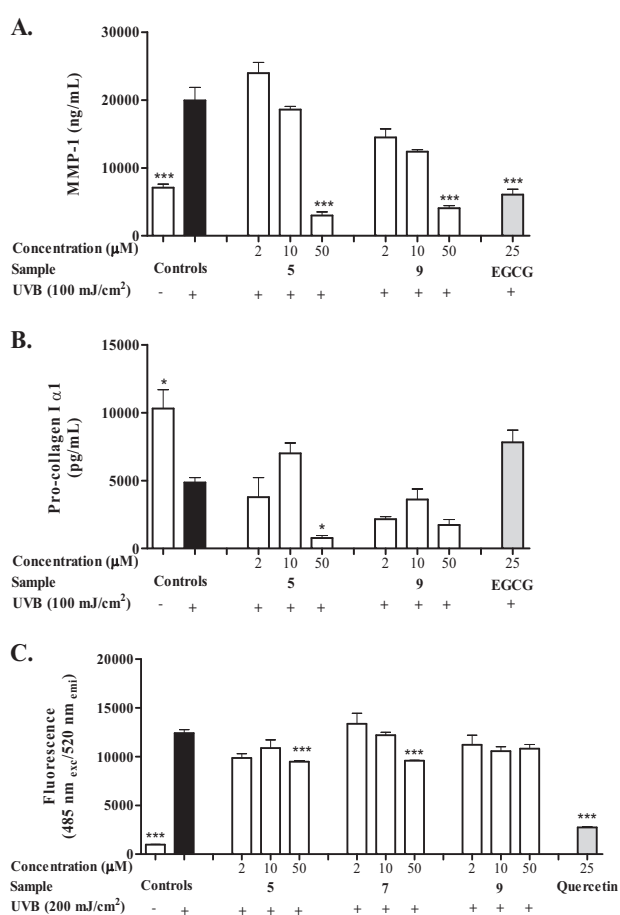


**Fig. 4** Photoprotective effects of potential quinoline-hydrazone hybrids on human dermal fibroblasts (HDF). Human MMP-1 and human procollagen were measured by ELISA after 100 mJ/cm<sup>2</sup> UVB irradiation. The results were normalized according to the percentage of viable cells determined by the WST-8 assay.  $1 \times 10^4$  HDF were treated with samples for 24 h. **a** After 72 h of irradiation, MMP-1 was measured and **b** 24 h after irradiation, procollagen I α1 was measured. **c** To quantify ROS production,  $5 \times 10^4$  cells were cotreated with samples for 2 h and then exposed to UVB (200 mJ/cm<sup>2</sup>) radiation. ROS generation was measured by DCFH-DA. All data are shown as the mean  $\pm$  SD of three independent experiments. \* $P < 0.05$ , compared with the UVB-irradiated control

are shown in Fig. 4. Compounds **5** and **9** were chosen for photoprotectivity testing on the basis of preliminary data and because strategies used to combat the devastating effects of photoaging can focus on compounds acting with different mechanisms involved in its pathogenesis (Duque et al. 2017). It is important to mention that the test hybrids were nontoxic to the cells, even at the highest concentration tested (50 mM, data not shown).

The exposure of fibroblasts to UVB radiation increased MMP-1 production and decreased type I procollagen secretion, as shown Fig. 4a, b, in a dose- and time-dependent manner (data not shown). After UVB exposure, the increase in MMP-1 secretion was 1.5-fold that of the control, and the decrease in procollagen production was

~56% that of unirradiated cells. Pretreatment with hybrids **5** and **9** significantly decreased the MMP-1 production in HDF in a dose-dependent manner after UVB irradiation. Both compounds decreased the level of MMP-1 compared with that of irradiated cells, but hybrid **5** showed higher activity at the highest evaluated concentration than compound **9** (Fig. 4a). Therefore, the position of the benzyl-hydrazone moiety on the quinoline ring is a critical structural motif for modulating the production of MMP-1 in the cell bioassay. Interesting results were also obtained with the pretreatment of the reference compound EGCG (25  $\mu$ M). However, pretreatment with hybrid **5** (10  $\mu$ M) reduced the deleterious effect of UVB exposure on HDF through the increase of procollagen production in ~44% of irradiated cells. Nevertheless, the procollagen production by fibroblasts treated with hybrid **9** and higher concentrations of hybrid **5** could suggest a probable phototoxic effect of the compounds.

To determine whether the trihydroxybenzyl-hydrazone derivatives **5** and **9** decreased MMP-1 production and increased procollagen secretion by HDF after UVB exposure via an antioxidant effect, the modulation of ROS production after UVB exposure (200 mJ/cm<sup>2</sup>) was evaluated. The dihydroxybenzyl-hydrazone derivative **7** was also evaluated based on its powerful antioxidant activity. The results are shown in Fig. 4c. The HDF exposed only to UVB had a marked increase in fluorescence, indicative of an increase in ROS generation at the single-cell level. Hybrids **5**, **7**, and **9** decreased ROS production in HDF after UVB irradiation by between 20 and 30% when cells were treated with 2, 10, and 50  $\mu$ M of each compound. This effect was not dose dependent, except for compound **7**, which showed higher activity at the highest evaluated concentration. Inside cells, ROS oxidize nonfluorescent DCFH-DA derivatives to green fluorescent pigment DCF, and the level of fluorescence is used as a marker of cytosolic ROS (Pygmalion et al. 2010). However, it was previously reported that not all radical species oxidize DCFH; therefore, the DCF level is used as a marker of only some reduced oxygen species (Bilski et al. 2002). Although the ROS level is overestimated and cannot be considered an absolute level, this approach was found to be suitable for comparing the efficacy of quinoline-hydrazone hybrids at the cellular level and for building a performance scale for ROS scavenging during irradiation.

### In silico ADME properties and percutaneous absorption parameters

We calculated and analyzed various drug-like properties of the nine quinoline-hydrazone hybrids, and the data are summarized in Table 4. All compounds exhibited significant values for the parameters analyzed, showing good

drug-like characteristics within the range of 95% of the known reference drugs. None of the hybrids **1–9** showed a violation of Lipinski's rule of five and its variants, making them potentially promising agents in pharmacological investigations as antiaging drugs. The skin penetration of active ingredients used in cosmetics is affected by their physicochemical properties, such as molecular weight and the partition coefficient (*P*). Chemical compounds with high or low *P* values or molecular weights >500 Da are generally poorly absorbed through the skin (Bos and Meinardi 2000). Accordingly, the physicochemical parameters of drugs used as transdermal therapeutic systems have appropriate *P* values (log *P* = 1–3) and low molecular weights (<500 Da) (Higo 2007), because antiaging formulations require both the breaching of the lipophilic stratum corneum and the resorption into the aqueous central compartment of the systemic circulation (Wiedersberg and Guy 2014). The in silico ADMET predictions of the novel hybrids **1–9** revealed the strongest prospects for use in topical formulations for aging skin, displaying optimal log *P* values (in the range of 3.071–1.646) and molecular weights ranging from 291 to 323 Da.

To screen for compounds active against skin aging and that are able to cross the dermal layers at physiologically relevant concentrations, four fundamental pharmacokinetic parameters involved in the development of cosmetic antiaging formulations were calculated (Klimova et al. 2018). Then, the in silico predictions of physicochemical transdermal properties for the hybrids **1–9** were investigated. The results indicated that all hybrids showed a skin permeation coefficient value (calculated by PreADMET 2.0 tool) comparable with some conventional topical drugs (ranging from –1.262 to –3.931) ranging between –1.754 and –3.524 and exhibited optimal values for percutaneous absorption (Log *P*<sub>ab</sub>), effective diffusion coefficient in dermis (*D*<sub>de</sub>) and maximum percutaneous flux (*J*<sub>max</sub>) corresponding to an effective transdermal permeability with high potential for percutaneous penetration. In addition, the pharmacokinetic parameters obtained from the in silico prediction suggest that, among all the tested compounds, hybrids **5** and **9** have promising antiaging activity because they displayed optimal partition and diffusion values into skin within the ideal range of the known typical drugs that are FDA-approved for transdermal administration.

All tests carried out in this study attempted to address a number of important molecular targets in the cascade of reactions that develop during photoaging, which interact with some quinoline-hydrazone hybrids. These hybrids are expected to possess diverse pharmacological activities in the pathological process of aging that involves multiple pathways. The combination of specific antioxidant and enzymatic inhibition activities was applied to the preliminary screening of the bioactive antiaging hybrids.

**Table 4** In silico physicochemical pharmacokinetic parameters of the synthesized hybrids **1–9**

Entry	M.W <sup>a</sup>	TPSA (7–200 Å <sup>2</sup> )	n-Rot Bond (<10)	n-ON <sup>c</sup> (<10)	n-OHNH <sup>d</sup> (<5)	Log P <sub>ow</sub> <sup>e</sup> (-2.0 –6.5)	Log S <sub>w</sub> <sup>f</sup> (-6 –0.5)	Predicted dermatopharmacokinetic (DPK) descriptors			Lipinski rule of five (≤1)		
								Log K <sub>p</sub> <sup>g</sup> (cm/h)g	Log P <sub>ab</sub> <sup>h</sup> (cm/h)	D <sub>de</sub> (mm <sup>2</sup> /s) <sup>i</sup>		Log J <sub>max</sub> (mol/cm <sup>2</sup> /h) × 10 <sup>-10</sup>	J <sub>max</sub> <sup>j</sup> (μg/cm <sup>2</sup> /h)
1	291.309	81.439	5.0	2.0	4.25	3.071	-4.408	-1.754	-2.317	0.416	3.67	0.107	0
2	307.308	102.949	6.0	3.0	5.00	2.370	-4.089	-2.647	-2.912	0.405	1.82	0.056	0
3	307.308	104.121	6.0	3.0	5.00	2.316	-4.114	-2.820	-2.950	0.405	1.82	0.056	0
4	307.308	104.121	6.0	3.0	5.00	2.316	-4.114	-2.820	-2.950	0.405	1.82	0.056	0
5	323.307	124.458	7.0	4.0	5.75	1.677	-3.786	-3.539	-3.502	0.395	0.91	0.029	0
6	307.308	102.409	6.0	3.0	5.00	2.340	-4.121	-2.686	-2.933	0.405	1.82	0.056	0
7	307.308	103.582	6.0	3.0	5.00	2.285	-4.146	-2.860	-2.972	0.405	1.82	0.056	0
8	307.308	103.582	6.0	3.0	5.00	2.285	-4.146	-2.860	-2.972	0.405	1.82	0.056	0
9	323.307	123.919	7.0	4.0	5.75	1.646	-3.817	-3.579	-3.524	0.395	0.91	0.029	0

<sup>a</sup>Molecular weight of the molecule

<sup>b</sup>Polar surface area (PSA) (7.0–200.0)

<sup>c</sup>n-ON number of hydrogen bond acceptors

<sup>d</sup>n-OHNH number of hydrogen bond donors

<sup>e</sup>Predicted octanol–water partition coefficient (log P<sub>ow</sub>) (-2.0 to 6.5)

<sup>f</sup>Predicted of solute aqueous solubility (Log S<sub>w</sub>) (-6.5 to 0.5)

<sup>g</sup>Skin permeation coefficient of chemical in the stratum corneum

<sup>h</sup>Percutaneous absorption M.W and Log P<sub>ow</sub>-based

<sup>i</sup>Effective diffusion coefficient in dermis M.W-based

<sup>j</sup>Solute maximum percutaneous flux across human skin (J<sub>max</sub>)

Later, a cell-based study of bioactive compounds verified the modulation of UVB-induced MMP-1 production and the inhibition of the suppression of type I procollagen synthesis mediated by the inhibition of the production of ROS in cultured HDF. Our results suggest that the activity of these hybrids as inhibitors of skin aging-related enzymes is associated to the number and position of the hydroxyl groups on the benzyl-hydrazone moiety. In addition, the antioxidant activities of the hybrids **5** and **9** are responsible for the cellular resistance to photoaging. However, it is possible that these hybrids may differentially affect various cellular signal cascades. Thus, further studies need to be conducted to validate the results of the in vitro assay.

## Conclusion

In summary, nine hybrids corresponding to two chemical series, 2- and 4-quinoline-hydrazones, were prepared and evaluated for their antiaging activities. The trihydroxylated quinoline-hydrazones **5** and **9** showed the best collagenase inhibition ( $IC_{50} = 39.4$  and  $45.6 \mu M$ , respectively). Compound **5** also showed significant activity against elastase and hyaluronidase ( $IC_{50} = 164.2$  and  $318.8 \mu M$ , respectively), and it was even better than the usual standard, i.e., commercial oleanolic acid ( $IC_{50} = 193.6 \mu M$  for elastase). This establishes the importance of the number and position of hydroxyl groups on the benzyl-hydrazone moiety. Molecular docking results suggest that the difference of inhibition between **5** and **9** is principally attributed to the hydrogen bonds interactions related to the residues His218 and His228 and Zn atom in collagenase, Val216 in elastase and Tyr75 for hyaluronidase. The quinoline-hydrazones **5**, **7**, and **9** showed different extents of radical-scavenging abilities against peroxy radicals that cause oxidative degradation, as detected with the ORAC test. In addition, the most potent compounds, quinoline-hydrazone **5** and **9**, significantly suppressed UVB-induced MMP-1 expression and inhibited the suppression of type I procollagen synthesis by inhibiting the production of ROS in cultured HDF. Overall, the occurrence of the quinoline hydrazone moiety presents interesting antiaging activity. The in silico results showed that all the tested hybrids **1–9** could be suitable in formulations for efficient drug delivery to the skin and displayed good skin permeation properties. Therefore, our study presented advantageous results for antiaging drug discovery focused on quinoline-hydrazone hybrids as dual inhibitors of skin aging-related enzymes, as antioxidants and as inhibitors of the biological effects of UVB irradiation. Further studies are necessary to elucidate the mechanisms by which hybrids block the effects of UVB irradiation on an in vivo model.

**Acknowledgements** This investigation received financial support from Universidad de Antioquia, UdeA.

## Compliance with ethical standards

**Conflict of interest** The authors declare that they have no conflict of interest.

**Publisher's note:** Springer Nature remains neutral with regard to jurisdictional claims in published maps and institutional affiliations.

## References

- Adamo C, Barone V (1999) Toward reliable density functional methods without adjustable parameters: the PBE0 model. *J Chem Phys* 110:6158–6170
- Belkheiri N, Bouguerme B, Bedos-Belval F, Duran H, Bernis C, Salvayre R, Nègre-Salvayre A, Baltas M (2010) Synthesis and antioxidant activity evaluation of a syringic hydrazones family. *Eur J Med Chem* 45:3019–3026
- Bilski P, Belanger AG, Chignell CF (2002) Photosensitized oxidation of 2',7'-dichlorofluorescein: singlet oxygen does not contribute to the formation of fluorescent oxidation product 2',7'-dichlorofluorescein. *Free Radic Biol Med* 33:938–946
- Bos JD, Meinardi MM (2000) The 500 Dalton rule for the skin penetration of chemical compounds and drugs. *Exp Dermatol* 9:165–169
- Bravo K, Alzate F, Osorio E (2016) Fruits of selected wild and cultivated Andean plants as sources of potential compounds with antioxidant and anti-aging activity. *Ind Crop Prod* 85:341–352
- Bravo K, Duque L, Ferreres F, Moreno DA, Osorio E (2017) *Passiflora tarminiana* fruits reduce UVB-induced photoaging in human skin fibroblasts. *J Photochem Photobiol B Biol* 168:78–88
- Bravo K, Sepulveda-Ortega S, Lara-Guzman O, Navas-Arboleda AA, Osorio E (2015) Influence of cultivar and ripening time on bioactive compounds and antioxidant properties in Cape gooseberry (*Physalis peruviana* L.). *J Sci Food Agric* 95:1562–1569
- Cătană CS, Atanasov AG, Berindan-Neagoe I (2018) Natural products with anti-aging potential: affected targets and molecular mechanisms. *Biotechnol Adv* 36:1649–1656
- Chaaban I, Rizk OH, Ibrahim TM, Henen SS, El-Khawass EM, Bayad AE, El-Ashmawy IM, Nematalla HA (2018) Synthesis, anti-inflammatory screening, molecular docking, and COX-1,2/5-LOX inhibition profile of some novel quinoline derivatives. *Bioorg Chem* 78:220–235
- Chao KL, Muthukumar L, Herzberg O (2007) Structure of human hyaluronidase-1, a hyaluronan hydrolyzing enzyme involved in tumor growth and angiogenesis. *Biochemistry* 46:6911–6920
- Chen L, Han L, Saib O, Lian G (2015) In silico prediction of percutaneous absorption and disposition kinetics of chemicals. *Pharm Res* 32:1779–1793
- Choudhary S, Singh PK, Verma H, Singh H, Silakari O (2018) Success stories of natural product-based hybrid molecules for multifactorial diseases. *Eur J Med Chem* 151:62–97
- Coa JC, Castrillón W, Cardona W, Carda M, Ospina V, Muñoz JA, Vélez ID, Robledo SM (2015) Synthesis, leishmanicidal, trypanocidal and cytotoxic activity of quinoline-hydrazone hybrids. *Eur J Med Chem* 101:746–753
- Coa JC, García E, Carda M, Agut R, Vélez ID, Muñoz JA, Yepes LM, Robledo SR, Cardona W (2017) Synthesis, leishmanicidal, trypanocidal and cytotoxic activities of quinoline-chalcone and quinoline-chromone hybrids. *Med Chem Res* 26:1405–1414
- Czarnicka K, Girek M, Maciejewska K, Skibiński R, Jończyk J, Bajda M, Kabziński J, Sołowiej P, Majsterek I, Szymański P (2017)

- New cyclopentaquinoline hybrids with multifunctional capacities for the treatment of Alzheimer's disease. *J Enzyme Inhib Med Chem* 33:158–170
- de Heer MI, Mulder P, Korth HG, Ingold KU, Luszyk J (2000) Hydrogen atom abstraction kinetics from intramolecularly hydrogen bonded ubiquinol-0 and other (poly)methoxy phenols. *J Am Chem Soc* 122:2355–2360
- Dimitrijević J, Cvetković D, Radovanović A, Nikolić V, Radovanović B (2016) Photolytic behaviour of 1h-indole-2,3-dione 3-[(2,4-dinitrophenyl)hydrazone and 2-hydroxy-4-methoxybenzophenone. *Adv Technol* 5:27–32
- Duque L, Bravo K, Osorio E (2017) A holistic anti-aging approach applied in selected cultivated medicinal plants: a view of photoprotection of the skin by different mechanisms. *Ind Crop Prod* 97:431–439
- El-Feky SA, Abd El-Samii ZK, Osman NA, Lashine J, Kamel MA, Thabet HKh (2015) Synthesis, molecular docking and anti-inflammatory screening of novel quinoline incorporated pyrazole derivatives using the Pfitzinger reaction II. *Bioorg Chem* 58:104–116
- Farrokhnia M, Mahnam K (2017) Molecular dynamics and docking investigations of several zoanthamine-type marine alkaloids as matrix metalloproteinase-1 inhibitors. *Iran J Pharm Res* 16:173–186
- Franck X, Fournet A, Prina E, Mahieux R, Hocquemiller R, Figadère B (2004) Biological evaluation of substituted quinolones. *Bioorg Med Chem Lett* 14:3635–3638
- Freitas-Rodríguez S, Folgueras AR, López-Otín C (2017) The role of matrix metalloproteinases in aging: tissue remodeling and beyond. *BBA Mol Cell Res* 1864:2015–2025
- Frisch MJ, Trucks GW, Schlegel HB, Scuseria GE, Robb MA, Cheeseman JR et al. (2009) Gaussian 09. Revision A.1, Gaussian, Inc., Wallingford CT
- Haywood R, Rogge F, Lee M (2008) Protein, lipid, and DNA radicals to measure skin UVA damage and modulation by melanin. *Free Radic Biol Med* 44:990–1000
- Higo N (2007) Recent trend of transdermal drug delivery system development. *Yakugaku Zasshi* 127:655–662
- Hohl CM, Dankoff J, Colacone A, Afilalo M (2001) Polypharmacy, adverse drug-related events, and potential adverse drug interactions in elderly patients presenting to an emergency department. *Ann Emerg Med* 38:666–671
- Kang SM, Han S, Oh JH, Lee YM, Park CH, Shin CY, Lee DH, Chung JH (2017) A synthetic peptide blocking TRPV1 activation inhibits UV-induced skin responses. *J Dermatol Sci* 88:126–133
- Klimova B, Novotny M, Kuca K (2018) Anti-aging drugs—prospect of longer life? *Curr Med Chem* 25:1946–1953
- Kumar V, Basavarajaswamy G, Rai MV, Poojary B, Pai VR, Shruthi N, Bhat M (2015) Rapid 'one-pot' synthesis of a novel benzimidazole-5-carboxylate and its hydrazone derivatives as potential anti-inflammatory and antimicrobial agents. *Bioorg Med Chem Lett* 25:1420–1426
- Kumud M, Sanju N (2018) In-vitro evaluation of antioxidant, anti-elastase, anti-collagenase, anti-hyaluronidase activities of safranal and determination of its sun protection factor in skin photoaging. *Bioorg Chem* 77:159–167
- Lovejoy B, Cleasby A, Hassell AM, Longley K, Luther MA, Weigl D, McGeehan G, McElroy AB, Drewry D, Lambert MH, Jordan SR (1994) Structure of the catalytic domain of fibroblast collagenase complexed with an inhibitor. *Science* 263:375–377
- Marella A, Tanwar OP, Saha R, Ali MR, Srivastava S, Akhter M, Shaquiquzzaman M, Alam MM (2013) Quinoline: a versatile heterocyclic. *Saudi Pharm J* 21:1–12
- Masak H (2010) Role of antioxidants in the skin: Anti-aging effects. *J Dermatol Sci* 58:85–90
- Morris GM, Goodsell DS, Halliday RS, Huey R, Hart WE, Belew RK, Olson AJ (1998) Automated docking using a Lamarckian genetic algorithm and an empirical binding free energy function. *J Comput Chem* 19:1639–1662
- Morris GM, Huey R, Lindstrom W, Sanner MF, Belew RK, Goodsell DS, Olson AJ (2009) AutoDock4 and AutoDockTools4: automated docking with selective receptor flexibility. *J Comput Chem* 30:2785–2791
- Mukherjee PK, Bahadur S, Chaudhary SK, Harwansh RK, Nema NK (2015) Validation of medicinal herbs for skin aging. In: Mukherjee PK (ed) Evidence-Based Validation of Herbal Medicine. Elsevier Inc, Amsterdam, p 119–147
- Mukherjee PK, Maity N, Nema NK, Sarkar BK (2011) Bioactive compounds from natural resources against skin aging. *Phytomedicine* 19:64–73
- Ndlovu G, Fouche G, Tselanyane M, Cordier W, Steenkamp V (2013) In vitro determination of the anti-aging potential of four southern African medicinal plants. *BMC Complement Altern Med* 13:304
- Newton MD (1969) Self-consistent molecular-orbital methods. II. Projection of diatomic differential overlap (PDDO). *J Chem Phys* 51:3917–3926
- Nurkenov OA, Satpaeva ZhB, Schepetkin IA, Khlebnikov AI, Turdybekov KM, Seilkhanov TM, Fazylov SD (2017) Synthesis and biological activity of hydrazones of o- and p-hydroxybenzoic acids. Spatial structure of 5-bromo-2-hydroxybenzylidene-4-hydroxybenzohydrazide. *Russ J Gen Chem* 87:2299–2306
- Parkinson CJ, Mayer PM, Radom L (1999) An assessment of theoretical procedures for the calculation of reliable radical stabilization energies. *J Chem Soc Perkin Trans* 2:305–2313. 1999
- Parr RG, Szentpály L, Liu S (1999) Electrophilicity index. *J Am Chem Soc* 121:1922–1924
- Popiolek L (2017) Hydrazone-hydrazones as potential antimicrobial agents: overview of the literature since 2010. *Med Chem Res* 26:287–301
- Prior RL, Wu X, Schaich K (2005) Standardized methods for the determination of antioxidant capacity and phenolics in foods and dietary supplements. *J Agric Food Chem* 53:4290–4302
- Pygmalion MJ, Ruiz L, Popovic E, Gizard J, Portes P, Marat X, Lucet-Levannier K, Muller B, Galey JB (2010) Skin cell protection against UVA by Sideroxyl, a new antioxidant complementary to sunscreens. *Free Radic Biol Med* 49:1629–1637
- Ryu A, Arakane K, Koide C, Arai H, Nagano T (2009) Squalene as a target molecule in skin hyperpigmentation caused by singlet oxygen. *Biol Pharm Bull* 32:1504–1509
- Schoellhammer CM, Blankschtein D, Langer R (2014) Skin permeabilization for transdermal drug delivery: recent advances and future prospects. *Expert Opin Drug Deliv* 11:393–407
- Şenkardes S, Kaushik-Basu N, Durmaz İ, Manvar D, Basu A, Atalay R, Küçükgülzel ŞG (2016) Synthesis of novel diflunisal hydrazone-hydrazones as anti-hepatitis C virus agents and hepatocellular carcinoma inhibitors. *Eur J Med Chem* 10:301–308
- Singh M, Raghav N (2011) Biological activities of hydrazones: a review. *Int J Pharm Pharm Sci* 3:26–32
- Sivamani P, Singaravelu G, Thiagarajan V, Jayalakshmi T, Kumar G (2012) Comparative molecular docking analysis of essential oil constituents as elastase inhibitors. *Bioinformation* 8:457–460
- Suresh K, Sandhya B, Himanshu G (2009) Biological activities of quinoline derivatives. *Mini Rev Med Chem* 9:1648–1654
- Vergara S, Carda M, Agut R, Yepes LM, Vélez ID, Robledo SM, Cardona-G W (2017) Synthesis, antiprotozoal activity and cytotoxicity in U-937 macrophages of triclosan–hydrazone hybrids. *Med Chem Res* 26:3262–3273
- Verma G, Marella A, Shaquiquzzaman M, Akhter M, Ali MR, Alam MM (2014) A review exploring biological activities of hydrazones. *J Pharm Bioallied Sci* 6:69–80

- Wiedersberg S, Guy RH (2014) Transdermal drug delivery: 30+ years of war and still fighting! *J Control Release* 190:150–156
- Würtele M, Hahn M, Hilpert K, Höhne W (2000) Atomic resolution structure of native porcine pancreatic elastase at 1.1 Å. *Acta Cryst D* 56:520–523
- Yadagiri B, Holagunda UD, Bantu R, Nagarapu L, Guguloth V, Polepally S, Jain N (2014) Rational design, synthesis and anti-proliferative evaluation of novel benzosuberone tethered with hydrazide–hydrazones. *Bioorg Med Chem Lett* 24:5041–5044
- Yilmaz AD, Coban T, Suzen S (2012) Synthesis and antioxidant activity evaluations of melatonin-based analogue indole-hydrazide/hydrazone derivatives. *J Enzym Inhib Med Chem* 27:428–436
- Zeng HJ, Yang R, You J, Qu LB, Sun YJ (2016) Spectroscopic and Docking Studies on the Binding of Liquiritigenin with Hyaluronidase for Antiallergic Mechanism. *Scientifica* 2016:1–8
- Zhang C, Wen C, Lin J, Shen G (2015) Protective effect of pyrroloquinoline quinine on ultraviolet A irradiation-induced human dermal fibroblast senescence in vitro proceeds via the anti-apoptotic sirtuin 1/nuclear factor-derived erythroid 2-related factor 2/heme oxygenase 1 pathway. *Mol Med Rep* 12:4382–4388